The Interaction of Proton Irradiation with Zr Textured Microstructure

DOI:
10.1016/j.jnucmat.2021.152808

Document Version
Final published version

Journal of Nuclear Materials 547 (2021) 152808

Contents lists available at ScienceDirect

Journal of Nuclear Materials

journal homepage: www.elsevier.com/locate/jnucmat

The interaction of proton irradiation with Zr textured microstructure

A. Adrych-Brunning*, C.P. Race

School of Materials, University of Manchester, Manchester, M13 9PL England

ARTICLE INFO

Article history:
Received 5 September 2020
Revised 11 December 2020
Accepted 10 January 2021
Available online 21 January 2021

Keywords:
Zirconium
Texture
Channelling
Proton irradiation
Damage quantification
TEM

ABSTRACT

Proton irradiation is commonly used as a surrogate for neutrons in experimental studies of structural materials for thermal reactors, such as Zr alloys. The proton beam is unidirectional which requires a choice to be made about the direction of the beam relative to the sample. The direction of the proton beam will determine what lattice orientations the protons will predominantly interact with, particularly in a sample with a strong texture. Since protons can be channelled the orientation of the crystal will affect the energy deposition and the implantation range. We have therefore investigated the degree of high energy proton channelling in crystal orientations found in a strongly textured sample of Zr. We find that the crystal orientations near low-index crystal directions like the $\langle 1\,1\,\bar{2}\,0\rangle$ zone axis encourage a higher degree of proton channelling compared with other crystal orientations commonly found in a split-basal textured sample. Channelling in these orientations can change the energy deposition of protons by 40%. Our results show that care must be taken when quantifying the damage in textured samples using a single grain orientation. To compensate for channelling effects, the damage from ion irradiation in a textured sample should be quantified by averaging the damage across many different grain orientations, especially when the irradiation temperature of the bulk is less than 300 K.

1. Introduction

Zr alloys are used as cladding material for the fuel in thermal reactors. Under deformation Zr is susceptible to strong texture development [1], which means that Zr materials develop anisotropic mechanical properties. The processing route used to deform Zr polycrystalline samples determines the preferential orientation of the basal poles. The basal poles typically align parallel with the direction of the compressive forces applied during processing. The high wall thickness and low diameter [1] created from the pilgering process [2,3] for cladding used in nuclear reactors results in the final stable texture known as split-basal texture. This texture includes a large fraction of the grains in a polycrystalline sample with the [0 0 0 1] crystal orientation pointing parallel with the radial direction of the tube with up to $\pm 40^{\circ}$ tilt towards the tangential direction (TD) of the tube. The texture created by the pilgering process can be reproduced using sheet rolling [1] in the lab, but the basal poles are instead parallel with the normal direction (ND) of the sample, which is perpendicular to the rolling direction. The ND of the sheet then represents the radial direction of the cladding tube in the lab.

Study of the failure mechanisms of reactor materials would ideally involve experimental analysis after neutron irradiation, however sources of neutrons are scarce and expensive, the samples are active and it can take years for property changes and failures to appear in neutron-irradiated materials, hence the renewed interest in using proton irradiation as a surrogate for neutron irradiation experiments.

In our analysis and discussion we will consider a typical experimental approach in which the proton beam direction (Fig. 1(a)) is aligned with the ND of the rolled sheet, but we note that similar arguments would apply to any choice of sample orientation with respect to the proton beam.

Whilst the crystal orientation is unlikely to have an effect on the energy deposited by neutrons, due to the low thermal collision cross-section of neutrons and the many directions that the neutrons travel in the reactor, the crystal orientation could however affect the energy deposited by protons because of channelling.

Channelling is a well known phenomenon whereby an ion travels along an open channel in the crystal lattice. The open channel reduces the strength of the interactions between the ion and the crystal lattice. The channelled ion will undergo only small angle scattering reducing the energy lost by the ion compared with an ion travelling along a random crystal direction. The reduced rate of energy loss increases the distance that the ion will travel into the material (the penetration depth) before implanting (Fig. 1(c)).

* Corresponding author.
E-mail addresses: aadrychbrunning@gmail.com (A. Adrych-Brunning), christopher.race@manchester.ac.uk (C.P. Race).

https://doi.org/10.1016/j.jnucmat.2021.152808

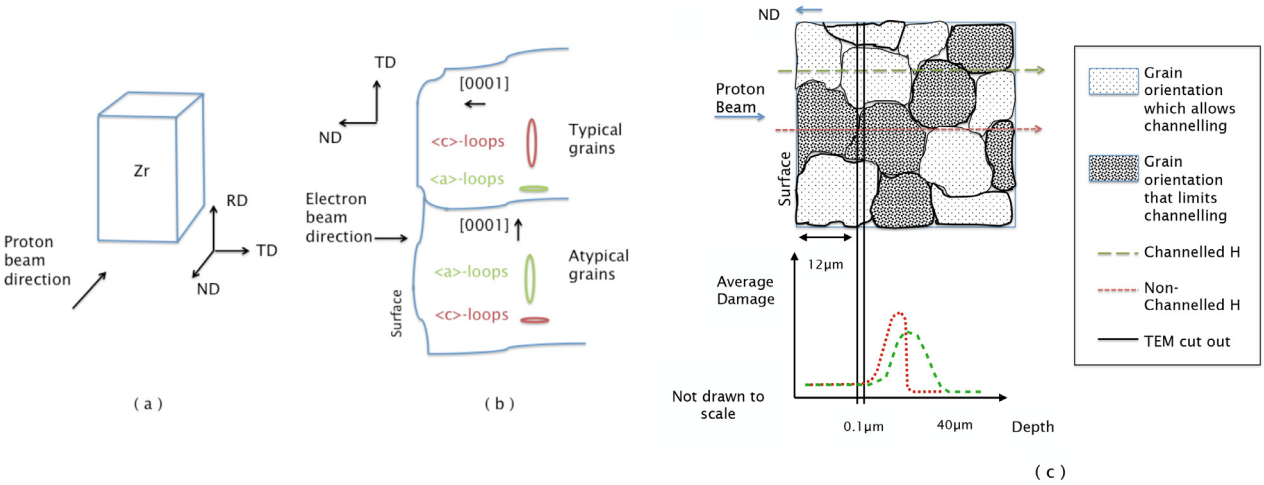

Fig. 1. A schematic of (a) the proton irradiation direction of a rolled Zr polycrystalline sample and (b) the typical dislocation loop distribution within a single transmission electron microscope (TEM) foil. A *c*-loop (a dislocation loop that lies on the basal plane) appears as a loop when the typical grain orientation (the [0 0 0 1] crystal orientation within 40° of the ND of the sample) is parallel with the electron beam direction, whereas an *a*-loop (a dislocation loop that lies on the prismatic plane) would appear as a line and vice versa when the [0 0 0 1] crystal orientation is rotated (atypical grains with the [0 0 0 1] crystal orientation tilted $\geq 70^{\circ}$ from the ND of the sample), when the c/a ratio $<$ ideal. (c) is a schematic of the predicted change in Bragg peak as a result of ions travelling within grains (of typical size 15 μm [4]) whose crystal orientation encourages channelling (green dashed line) compared with an ion travelling through a grain whose crystal orientation does not encourage channelling (red dashed line) in a polycrystalline sample. The solid black line shows the region in which a TEM foil is taken for experimental observation. The TEM foil is taken from the 60% depth from the Bragg peak position, which would typically be calculated assuming an amorphous structure in the program Stopping and Range of Ions in Matter (SRIM [5]). (For interpretation of the references to color in this figure legend, the reader is referred to the web version of this article.)

Channelling directions can be determined experimentally by observing the change in the Bragg peak distribution as a function of the angle of incidence of a beam of ions along different crystal directions [6–8].

The first computer simulation to demonstrate channelling was developed by Oen and Robinson [9] who numerically solved the scattering angle integral to find the energy lost by an ion as it travelled through a lattice, using the binary collision approximation (BCA). The authors found that the distance that the ion travelled in a lattice changed with the initial direction of the ion. Ions in an fcc lattice travelled further along the [0 1 1] crystal direction compared with the [0 0 1] crystal direction and an ion travelling along the [1 1 1] bcc crystal direction would travel further than if it travelled along the [0 0 1] crystal direction.

Recent developments in computer simulations mean that the crystal directions that encourage channelling can be identified. For example, Nordlund et al. [10] developed the program MDRANGE [11] which employs a simplified molecular dynamics (MD) approach to ion interactions using a recoil interaction approximation (RIA). Whilst a classical MD simulation calculates the forces between all the atoms in the system and then integrates the equations of motion to calculate the positions and velocities of all the atoms, the developers of MDRANGE limit the force calculation to only a recoiling ion ($E \geq$ 1keV) and its nearest neighbours. By significantly reducing the number of force calculations the speed of the simulation is increased which makes more feasible range-distribution calculations for high energy ions and the broad sampling of lattice orientations required in channelling simulations to find open channels. However by limiting the number of atoms included in the force calculation, effects of more distant atoms in the lattice are ignored, including the dissipation of heat through atomic vibrations generated along the ion's trajectory into the lattice.

Using MDRANGE the authors of Ref. [10] explored a series of beam and lattice orientations to find that the dominant channelling directions for 10 keV Zr ions into Zr were along the [0 0 0 1] and $\left[\bar{1}\,2\,\bar{1}\,0\right]$ directions in bulk Zr and that such channelling events can increase the maximal penetration depth of an ion by a factor of two compared with the same ions travelling along non-channelling directions.

Whilst channelling has been used in the experimental analysis of materials such as determining the occupational sites of defects in a lattice and the surface structure of the material [12], there has been little work that describes what effect channelling would have on ions, including protons, interacting with a polycrystalline sample with a strong texture.

After irradiating a sample with protons the irradiation-induced changes in the microstructure can be compared with the equivalent features in a neutron-irradiated sample using techniques like transmission electron microscopy (TEM) [13,14]. One common indication of irradiation damage in the material is the increase in the dislocation density in the sample. The change in the dislocation density is of particular interest in Zr alloys because of the role of dislocation loops in irradiation-induced growth (IIG) [15–18].

The dislocation loops can be observed using TEM by removing a thin foil from the bulk of the proton-irradiated material. The irradiated surface of the material is electro-polished [19] down to a predefined depth determined with respect to the position of the Bragg peak e.g. at 60% of the peak depth [19,20] and then is typically cut to be 100 nm thick and 3 mm wide. The position of the Bragg peak is most often calculated using the Monte Carlo program, Stopping and Range of Ions In Matter (SRIM [5]), which assumes an amorphous structure. For pure Zr the TEM foil is typically taken beyond 12 μm into the sample, shown by the solid black line in Fig. 1(c). This approach to sampling the irradiated material avoids the effect of surface damage as well as ignoring the region of implanted hydrogen. The foil can contain several different grains (the average grain size for Zircaloy-2 is 15 μm [4]). As shown in Fig. 1(c), the energy lost by protons can vary dependent on whether the protons interact with a grain whose crystal orientation encourages channelling or is "shielded" to different degrees by the grain above. The change in the energy lost therefore changes the position of the true Bragg peak. However the depth at which a TEM foil is cut from a sample is dependent on the Bragg peak as calculated by SRIM. Given the change in the Bragg peak as a result of ion channelling, the TEM foil could instead be cut from a high damage region (see

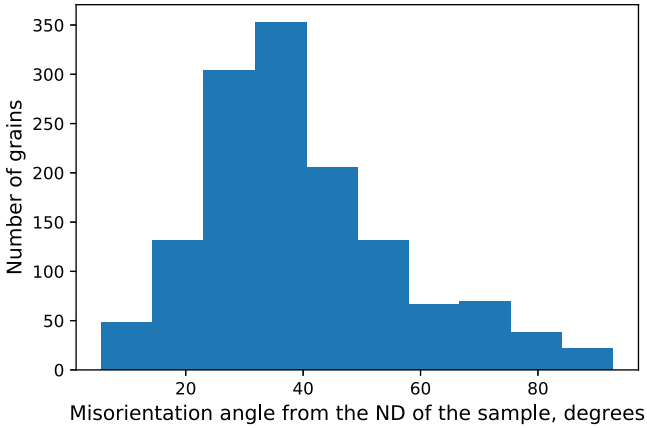

Fig. 2. A histogram of the number of grains in the Zircaloy-4 sample binned by the misorientation angle of the grain's [0 0 0 1] crystal direction from the ND of the sample [1].

the red dashed line in Fig. 1(c)) because of the protons travelling through grains whose orientation does not encourage channelling. As such more damage could be observed within the TEM foil than would be expected based on the calculation of the damage distribution using SRIM.

The crystal orientation has previously been found to affect the damage introduced by ion beams. Whilst the authors of Ref. [21] do not mention channelling specifically, they observed a change in the lattice hardness with the orientation of the crystal. The largest lattice hardness was near the basal plane orientation [10 $\bar{1}$ 3 0] which is assumed to be caused by an increase in the damage accumulation. The authors suggest that the orientations with low linear densities (number of atoms per unit cell length), like the [10 $\bar{1}$ 3 0] crystal orientation, have fewer atoms to disperse the momentum evenly. In terms of channelling this would mean that there would be fewer atoms within a channel that could constrain the ion within the channel. The ions are instead more likely to scatter off individual atoms within a channel and increase the number of displacements and damage in a grain.

In the following discussion we will assume that the TEM foil is cut so that its normal is aligned along the irradiation direction and hence also along the ND of the rolled plate (See Fig. 1(a)) according to our earlier assumption.

In a Zr polycrystalline material with a split-basal texture, the majority of the grains have the [0 0 0 1] crystal axis orientated within 40° of the ND of the sample (59.2% for recrystallized Zircaloy-4, see Fig. 2(b)), otherwise referred to as typical grains, which increases the probability of channelling based on Nordlund et al.'s results [10]. Since the proton beam is aligned parallel with the ND of the sample, the protons could deposit less energy in the typical grain orientations compared with atypical grain orientations and cause less damage to occur within the grains that encourage channelling or in those that are "shielded" by a non-channelling grain above.

A common experimental practice used to quantify the amount of damage in a sample is to count the number of *a*-loops. However, this is difficult to do in a grain with the [0 0 0 1] crystal direction perpendicular to the foil because the loops appear as small dots (short lines) as a result of their habit plane (see Fig. 1(b) [18]). In some foils the *a*-loops can be too numerous to distinguish from other defects [15]. The *a*-loop density can be more easily calculated from a grain that has its [0 0 0 1] crystal orientation tilted $\geq 70^{\circ}$ from the foil normal e.g. a grain with an orientation of $\left[1\bar{2}10\right]$ [19] close to parallel with the ND of the sample so that the *a*-loops appear as loops instead of dots (see Fig. 1(b)), which we refer to as an atypical grain.

Although *a*-loop counting is easier using a grain with the $\left[1\bar{2}10\right]$ crystal orientation parallel with the TEM foil normal, this will also be aligned with the ND in the original rolled plate and so the damage quoted for the entire sample is quantified using atypical grains rather than the more common grain orientations in the split-basal texture.[1]

As discussed above, protons may be channelled more in atypical grains than typical grain orientations. With less energy deposited in grains by channelled protons than non-channelled protons, the damage calculated using atypical grains would therefore underestimate the damage in the textured sample.

As such three questions arise. First, what degree of ion channelling occurs in Zr crystal orientations using 2 MeV protons typical of those used in irradiation experiments and second, what effect will channelling have on the possible damage distribution in the grain orientations found in a textured sample. Third, what, if any, biases might be introduced by counting loops under the constraints of TEM. This paper aims to answer these questions using molecular dynamics simulations of proton bombardment in Zr and discusses the implications for experimental TEM observations of dislocation loops with respect to proton and neutron irradiation.

2. Computational methods

As discussed above, channelling is a well known phenomenon whereby an ion travels along an open channel in the crystal lattice and loses less energy than a non-channelled ion because of the reduced strength of interactions between the ion and the crystal lattice. Channelling was originally described by Lindhard's continuum approximation [22] whereby a row of atoms can be described as a string and two-body collisions can be assumed between the incident ion and the string. The continuum potential, $U_i(\rho)$, due to the *i*th string,

$$U_i(\rho) = \int_{-\infty}^{\infty} \frac{\mathrm{d}z}{d_i} V(\sqrt{z^2+\rho^2}), \tag{1}$$

is calculated as an average of the atoms in the string, where ρ is the separation between the ion and the row of atoms, z is the distance along the row, d_i is the interplanar spacing between atoms in the row i and $V(\sqrt{z^2+\rho^2})$ is the interaction potential between the host atoms and the channelling species.

The continuum approximation assumes that the ion is only affected by the forces in the transverse plane, i.e. normal to the rows, and so the conditions for channelling can be described by differences in the ion's transverse energy, $E_{\perp}$,

$$E_{\perp} = U(\rho) + E\sin(\psi), \tag{2}$$

where ψ is the transverse angle between the ion's trajectory and the row of interest and E is the ion's kinetic energy. $U(\rho)$ is the sum over i row potentials and is written as

$$U(\rho) = \sum_i U_i(\rho_i) - U_{\min}, \tag{3}$$

where $U_{\min}$ is chosen so that $U(\rho)$ tends to zero in the middle of the channel.

If an ion's angle of incidence, ψ, is less than some critical value ψ_{crit} then the ion is channelled [22,23] and if an ion is separated by more than a critical approach distance, ρ_{crit}, from the nearest

[1] Note that though the sample for irradiation can be cut from the rolled plate with a different orientation and the TEM foil can be cut from the irradiated sample with a different orientation to those assumed here, an analogous effect would always be possible as a result of the uniaxial nature of proton irradiation and the constraints in observing loops in the TEM.

row the ion will oscillate within the channel and the row of atoms will continue to act as a continuum string. If however $E_{\perp}$ increases, the ion can overcome the continuum potential and scatter off individual atoms instead of the continuum string.

To predict active channels previous authors (e.g. Lindhard [22], Hobler et al. [24] and Nordlund et al. [10]) have used the screened Coulomb potential to describe the atom-ion interactions. In the present work we instead used an embedded atom method (EAM) potential developed by Christensen et al. [25] to describe the interatomic forces of interstitial H interacting with bulk Zr.

Using the molecular dynamics (MD) code LAMMPS (Large-scale Atomic/Molecular Massively Parallel Simulator [26]), the EAM potential was used to simulate the channelling of protons in Zr. A Ziegler-Biersack-Littmark (ZBL) potential was individually splined on to the Zr-H pair potential at 2.2 Å in the Zr-H EAM potential to model the repulsive forces expected for high energy collisions in scattering interactions. This is because at very small separations ($<$ 0.01 Å) there is a discontinuity in the EAM potential, this coupled with the steep gradient of the Zr-H EAM potential at small separations ($<$ 1Å) required the ZBL to be splined at a large separation. At separations $>$2.2 Å the original Zr-H EAM potential is used to describe the interatomic forces.

Whilst the interatomic forces described beyond the spline radius of 2.2 Å would have a significant effect if the calculation was performed beyond 1×10^{-10} s i.e. observing the formation of cascades or the implantation of hydrogen into zirconium, we were only interested in the interatomic forces at short range and high energy up to 1×10^{-15} s. Although a check was performed that the splined EAM potential did not affect the equilibrium properties of the Zr lattice, it is possible that using the splined EAM potential in this work to model the formation of cascades may be misleading.

Previous channelling simulations have used a periodic bulk simulation cell and so only a small number of crystal orientations could be simulated for a hcp crystal. The orientation of the beam with respect to the bulk then had to be varied by changing the angle of incidence [10]. In order to sample the full range of beam orientations, an angle of incidence of up to 85° with respect to the bulk surface normal had to be used.

Here we use a different approach using a variant of the spherical cluster method (SCM) previously described in Ref. [27]. The SCM is a convenient way to construct cells that allow us to simulate arbitrary crystal orientations and hence removes the need for variations of the angle of incidence of the ion beam to the sample surface. Due to the symmetry of the hcp crystal lattice only orientations within a fraction of the full solid angle need to be simulated to determine the effect of the crystal orientation on proton channelling. As such our simulated crystal orientations are as shown in Fig. 3.

The lattice vector along which the proton travels (vector $\vec{A}$) can be simulated by creating a sphere of Zr and rotating the sphere so that the crystallographic vector $\vec{A}$ is parallel with the z-axis of the external reference frame. The sphere is then cut along the $x-y$ plane of the external frame at the closest interplanar spacing to $z = 0$ for the rotated crystal, exposing a flat plane of the chosen crystal orientation to incident protons.

The sphere of crystal (with a radius of 264 Å) was reduced to a simulation box size of 258.72 Å × 336.06 Å × 268.68 Å (80 × 60 × 52 lattice units) in x, y and z with periodic boundaries applied in x and y and finite boundaries along the z-direction as shown in Fig. 4. Although there are interfaces at the x and y boundaries because of a mismatch of the lattice across the boundaries, the interfaces do not interfere with the implantation process because the protons do not cross the $x-y$ boundaries and there are no defects produced that traverse the boundary. A 25 Å deep vacuum exists above the crystal surface in which the 2 MeV H

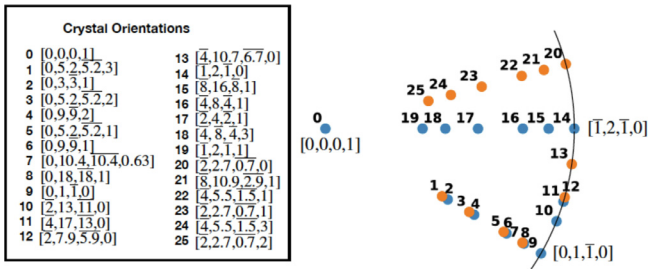

Fig. 3. A stereographic projection of the hcp crystal directions aligned parallel with the beam on to the (0 0 0 1) plane in Zr. The blue points show low-index directions and the orange points show high-index directions. (For interpretation of the references to color in this figure legend, the reader is referred to the web version of this article.)

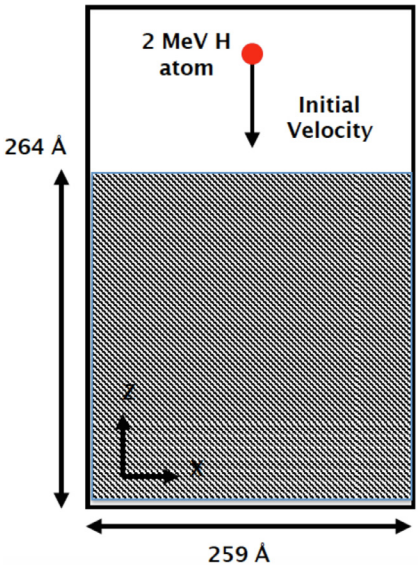

Fig. 4. A schematic of the simulation setup in LAMMPS. The crystal is orientated with respect to the reference frame so that the H atoms travel parallel with the chosen crystal direction from Fig. 3. The surface of the crystal is at $z = 0$.

atoms were introduced at 15 Å above the crystal surface, outside the range of the EAM potential.

The very high forces of the EAM potential at small separations mean that the movement of a high energy H atom at small separations from a Zr atom could only be captured with a very small time step of 1×10^{-5} femtoseconds.[2]

The EAM potential used in LAMMPS describes metallic bonding and therefore implicitly describes interactions between the nuclei and the majority of the effect of the electrons, but the potential does not include the non-adiabatic effects of nuclear-electron interactions. As discussed in previous papers [28–31] electronic interactions are important in metal simulations as the free electrons can conduct heat away from cascades. The electrons can also act as a reservoir that causes local heating and cooling of the ions via electronic excitations. These extra electronic interactions need to be explicitly included.

For fast moving ions ($\vec{v} \gg \vec{v}_0 Z_1^{2/3}$ where $\vec{v}_0$ is the Bohr velocity and Z_1 is the projectile's atomic number) the electronic loss can be approximated by applying a drag force equal to the electronic stopping force. For slow moving ions ($\vec{v} \ll 0.1\vec{v}_0$) the electronic interactions are described by an electron-phonon coupling which in-

[2] The default neighbour list cutoff was kept as the default value of 2.0 bins, with the neigh modify option check included to determine whether atoms have moved after every 10 steps in the simulation.

cludes the back and forth exchange of energy between the ions in the bulk and the electronic sub system. Whilst there are models that include both of these regimes such as the two temperature model (TTM) developed by Duffy et al. [32] or non-adiabatic models [28,33,34], these approaches are unnecessarily complicated for the fast light ions simulated here. The electronic losses can be approximated by removing energy from the H atoms via a simple drag force as mentioned above. Although the strength of the drag force will be dependent on the charge state of the channelling ion, the force can be approximated using SRIM [5]. SRIM [5] calculates the electronic stopping force of H using a fit to experimental data, hence the value of the stopping force will take into account any statistical distribution in the charge state of the H ion in Zr. For 2 MeV H in Zr, SRIM [5] calculates the electronic stopping to be 4.465 eV/Å. The drag force in LAMMPS is written as:

$$\vec{F}_{\text{stopping}} = -\gamma\vec{v} \tag{4}$$

Where $\vec{v}$ is the ion's velocity and γ is the drag coefficient, which in this case is 0.2198 molar mass/ps (in LAMMPS "metal" units). Although the electronic stopping force actually changes with the ion energy, a single value for the drag coefficient is justified by the small range of velocities exhibited by the channelling proton in our simulations

The complexity of the EAM potential compared with the screened Coulomb potential makes it difficult to find an analytical approximation to the interatomic potential for a row of atoms [23,24]. Without an approximation for the potential, the solution for the critical approach distance is difficult to obtain. This work instead finds the critical approach distance via direct simulation by sampling the surface of Zr bulk with a large number of proton implantations for different crystal orientations in order to find the separation, ρ, between the proton and a lattice row below which there is an increase in the energy lost by the proton as a result of high energy scattering events. This approach is based on Lindhard's discussion in Ref. [22] where the change in the energy lost by the ions in a thin film may be assumed to be dependent on the separation of the ion from the lattice atoms.

514 $x-y$ coordinate combinations were randomly generated within a box size of 239.32 Å × 358.46 Å (74 × 64 lattice units) and used as the entry points for the protons. Samples were pruned to ensure that each $x-y$ position was separated by at least 10 Å from other $x-y$ positions to reduce H-H interactions. For each proton, the perpendicular distance to every lattice atom, $\rho(i)$ was calculated as:

$$\rho(i) = \sqrt{(x_H - x_i)^2 + (y_H - y_i)^2}, \tag{5}$$

where x_H and y_H are the initial x and y coordinates of the proton and x_i and y_i are the x and y coordinates for the ith atom in the lattice. The smallest value of ρ, for lattice atoms with z-positions ≤200 Å from the surface, was then plotted as a function of the energy lost by each proton, after travelling 200 Å into a crystal.

The critical approach distance ρ_{crit} is the point at which there is a distinct change in energy lost by the protons. To find ρ_{crit}, each ρ, for all crystal orientations, was binned into 100 bins. Within each bin, an average was taken of the binned ρ to reduce the scatter. The ρ value at which the energy loss rate of protons exceeded the energy loss rate via electronic stopping (4.465 eV/Å) was identified as ρ_{crit}. The likelihood of proton channelling is then based on the value of ρ for each proton relative to ρ_{crit}, where if $\rho \geq \rho_{\text{crit}}$ the proton is considered to be channelled whereas if $\rho < \rho_{\text{crit}}$, the protons will undergo high energy scattering events. ρ_{crit} can then be regarded as the radius of a region around each row of atoms to distinguish regions of the lattice where protons are likely to be scattered or channelled.

Once ρ_{crit} was found, the energy lost by the protons in each crystal orientation was averaged over all protons to get an average energy loss for that orientation, where the energy loss includes the contribution from both electronic and nuclear interactions. The average energy loss was then compared with geometric features of the crystal orientation such as the occluded area fraction, linear density and the angular distribution of the orientation relative to the ND of the sample.

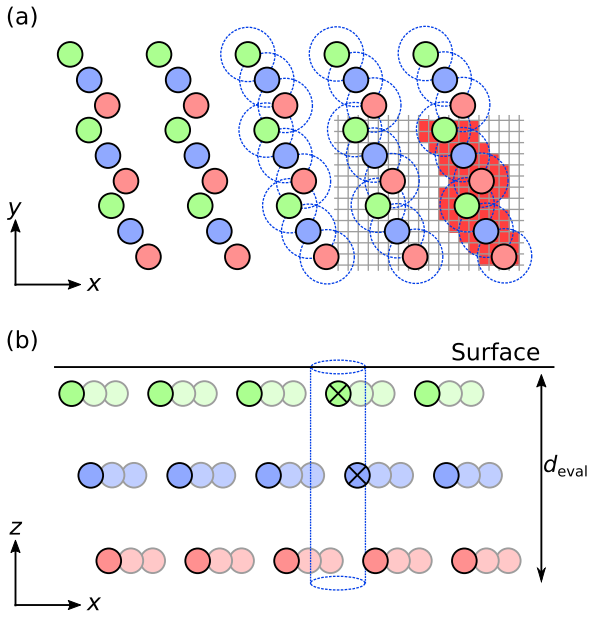

Fig. 5. A schematic illustration of the steps taken to calculate the occluded area fraction and the linear density for a given crystal orientation. (a) shows a view parallel to the initial proton direction and (b) a view normal to this, in which the sample surface is indicated. The filled circles mark the positions of atoms, with colours indicating different layers. Only those atoms within a distance d_{eval} of the surface are considered (in reality many more layers than shown are included within d_{eval}). In (a) we show the calculation of the occluded area fraction. We consider each atom to occlude an area of radius ρ_{crit} about its centre (shown by larger blue circles). We then consider a grid in the $x-y$ plane (in reality, much finer than shown) and squares whose centres fall within the ρ_{crit} are considered occluded (shown shaded red). In (b) we show the calculation of the linear density. A cylindrical volume of radius ρ_{crit} around an atom in the surface layer is considered (shown in blue). The number of atoms n falling within this cylinder (indicated by crosses) is calculated and the linear density is then given by n/d_{eval}. (For interpretation of the references to color in this figure legend, the reader is referred to the web version of this article.)

To calculate the occluded area fraction for a chosen crystal orientation, the fraction of the surface that is occluded by rows must be determined (see the schematic illustration in Fig. 5):

1. The atomic positions above an evaluation depth, d_{eval}, which in this work was taken as 100Å, were extracted from the simulation.
2. The extracted atomic positions were projected on to the xy plane.
3. For each unique xy atomic position, a screening centre was applied to each atom with radius equal to the calculated critical approach distance, ρ_{crit}. The screening centre represents the region outside of which a proton is channelled ($\rho \geq \rho_{\text{crit}}$) rather than scattered ($\rho < \rho_{\text{crit}}$).
4. The lattice surface was discretised with a grid, which in this case was 30 Å × 30 Å × 100 Å in $x-y-z$. The scale of the grid was chosen to be 0.1 Å; small enough to identify unique atomic positions in the lattice surface. Each grid point was checked to see if it fell within ρ_{crit} of an atom centre. If so, the grid point was counted as being occluded, shown as a red square in Fig. 5(a).
5. The fraction of occluded grid points is then the occluded area fraction.

To calculate the linear density of each string of atoms (Fig. 5(b)), the number of atoms whose single screening centres overlap was divided by d_{eval}. The linear density for each string was then averaged across all the strings within the evaluated surface.

The effect of channelling in a sample with a strong texture was also investigated by using the same method described above but constructing crystal orientations that were randomly sampled from a textured sample that contains a large fraction (59.2%) of grains with the [0 0 0 1] crystal axis tilted 40° from the ND of the sample and a small fraction of grains with the $[0\,1\,\bar{1}\,0]$ crystal direction aligned parallel with the TD of the sample.

As discussed above, there has been previous work by Nordlund on channelling in Zr [10] but the results were obtained using a simplified version of MD and with a low energy ion (10 keV Zr ion). To compare the results of Nordlund's model and this work, the implantation simulation was repeated using 10 keV protons and an input drag coefficient in Eq. (4) of 6.0724 molar mass/ps.

The Zr crystal in the 10 keV and 2 MeV simulations was at 0 K, but proton irradiation experiments are carried out at high temperatures (≥600 K) to roughly match the temperatures in a reactor, to accelerate the migration of clustered defects and to compensate for the high rate at which damage is introduced by proton irradiation compared with neutron irradiation. To observe the effect of temperature on the channelling of protons, the implantation simulations of the crystal orientations in Fig. 3 were repeated using simulation cells thermalised to 300 K, 600 K, 900 K and 1200 K using the Nosé-Hoover thermostat at fixed volume in LAMMPS for 10 picoseconds, with a time step of 10^{-5} fs. Once thermalised the thermostat was applied only to a 15 Å wide border around the bulk and the NVE integration was applied to the remaining atoms during the 2 MeV proton bombardment.

3. Results and discussion

3.1. Average energy loss

In Fig. 6 the energy lost by each simulated proton is plotted as a function of ρ to find $\rho_{crit} = 0.72$ Å, shown by the black line. At $\rho < 0.72$ Å the energy lost by the protons increases rapidly whereas the energy loss plateaus at $\rho \geq 0.72$ Å. The average energy lost by the protons travelling through each orientation of the Zr crystal is plotted on the stereographic projection in Fig. 7. The orientations were divided into subgroups based on the segments A-B-C-D in the stereographic projection. However there was no obvious pattern in the energy lost by the protons within each subgroup of the stereographic plot other than group D having an average energy loss that was 43% higher than A,B or C. This may be because there is a high number of high-index directions (shown in Fig. 3) within group D compared with A,B C. The orange points in Fig. 7 show a higher average energy loss than the blue points, because the orange points are fractionally higher index directions compared with the blue points.

Fig. 8 (a) shows that protons travelling through crystal orientations with a high occluded area fraction are more likely to lose a large amount of energy because there is less open space in the lattice in which the protons can be channelled. This becomes instantly apparent if the fraction of the occluded surface, including the screening centre, is plotted for the (d) [0 0 0 1] and (e) $[0\,18\,\bar{18}\,1]$ crystal orientations as in Fig. 8.

The low index crystal orientation [0 0 0 1] (Fig. 8(d)) has less space occluded by rows of atoms (and by the continuum potential of the row represented by the screening centre). Protons are therefore more likely to enter an open channel and be channelled compared with protons travelling in a high index crystal orientation like $[0\,18\,\bar{18}\,1]$ (Fig. 8(e)).

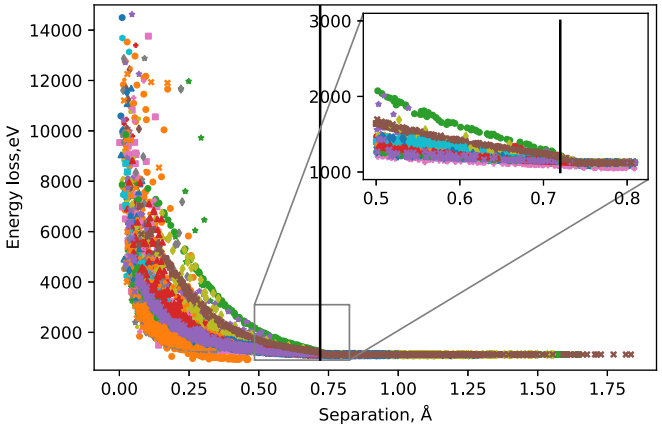

Fig. 6. The energy lost by 2 MeV protons after travelling 200 Å into a Zr crystal as a function of the separation between each proton and the closest lattice atom within each crystal orientation. Each point represents a single proton and each series one of the orientations shown in Fig. 3. The black line is the critical approach distance, $\rho_{crit} = 0.72$ Å.

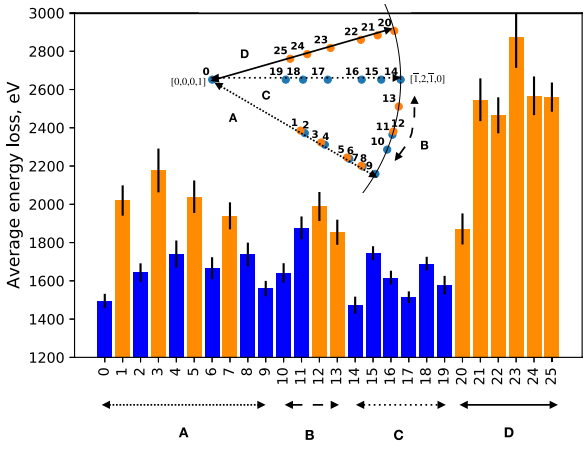

Fig. 7. The average energy lost by the protons travelling through a crystal with a given orientation grouped by the subset of the crystal orientation on the stereographic projection. The numbers follow the same distribution as that of Fig. 3. The error bars represent the standard error in the average energy lost by the protons for each orientation. The orange points distinguish marginally higher index directions than the blue points. (For interpretation of the references to color in this figure legend, the reader is referred to the web version of this article.)

For the high index crystal directions the lattice does not repeat until large depths in the material, and this results in the low linear density in Fig. 8(c). The authors of Ref. [21] theorised that the damage created by incoming ions was reduced if the crystal orientation had a high linear density because the momentum transferred by the scattering of ions along the channel was more evenly transferred in comparison with an orientation with a low linear density. This observation appears to be consistent with the observed trend in Fig. 8(b).

Since protons lose less energy when travelling through low index crystal orientations compared with high index crystal directions, there is less energy deposited in the lattice that can produce radiation-induced defects and hence changes in the microstructure such as the formation of dislocation loops. This suggests that there should be less microstructural changes in low index crystal orientations compared with high index crystal orientations. Of course, the processes leading to dislocation loop formation, for example, form over much longer timescales (1×10^{-10} s) than was studied in this work (1×10^{-15} s).

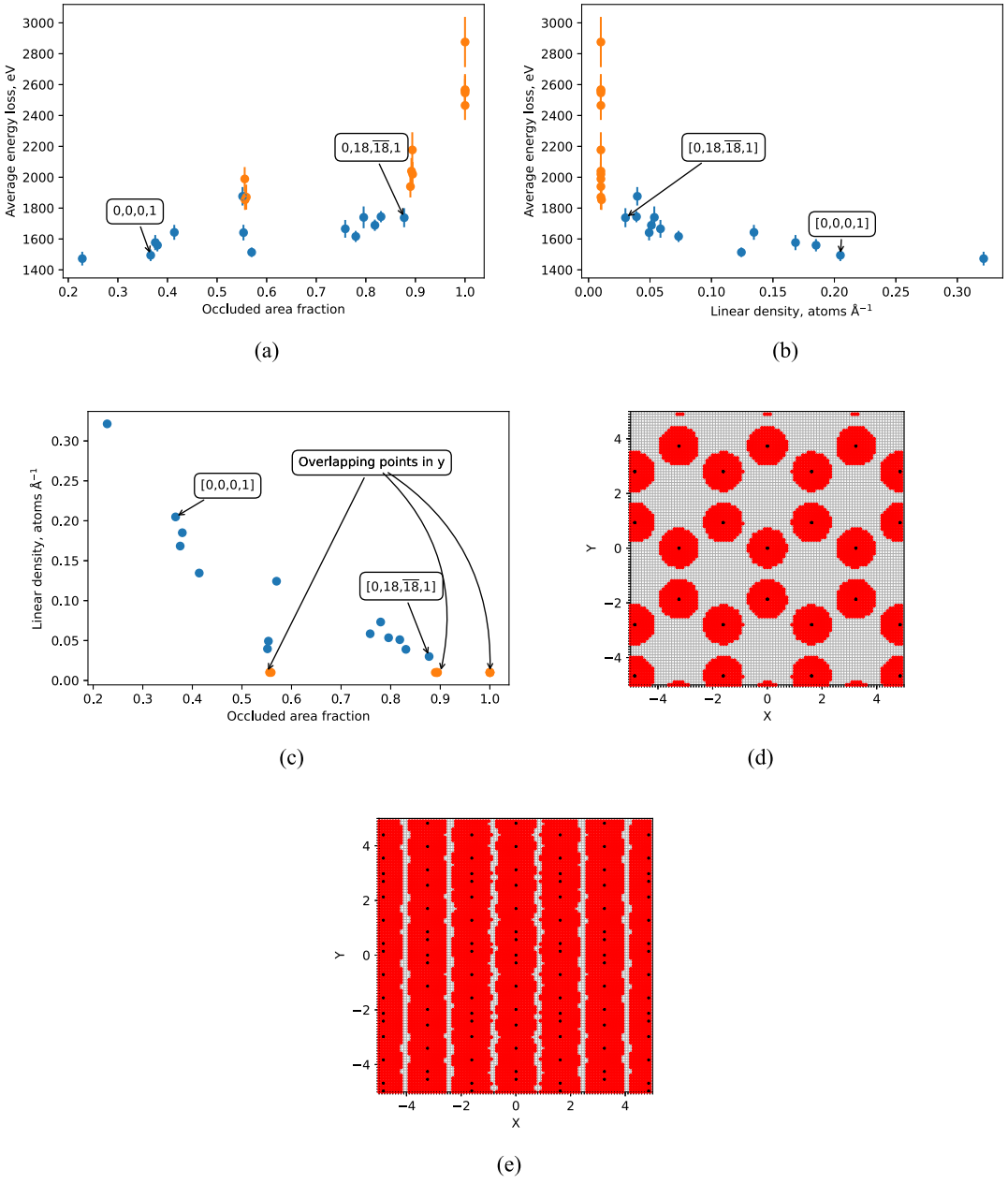

Fig. 8. For each crystal orientation the average energy lost by the protons is plotted as a function of (a) the occluded area fraction and (b) the linear density. The error bars are the standard error in the average energy lost by the protons. The linear density for each crystal orientation is plotted against the corresponding occluded area fraction in (c). The red circle around each lattice point (black points) represents the occluded area around a row of atoms within which scattering is likely to occur in the crystal orientations (d)[0 0 0 1] and (e) $\left[0\,18\,\overline{18}\,1\right]$. The grid lines in (d) and (e) show the distribution of the grid employed to calculate the occluded area fraction, as shown in the schematic in Fig. 5(b). (For interpretation of the references to color in this figure legend, the reader is referred to the web version of this article.)

The correlation between the occluded area fraction and the average energy lost by protons as a function of crystal orientation suggests that the occluded area fraction may be an easily calculated predictor of the degree of proton channelling with changing crystal orientation avoiding the need to calculate analytical solutions from channelling theory or to run full simulation dynamics.

3.2. Effect of texture

To study the effects of texture, we simulated the proton implantation for 166 crystal orientations randomly sampled from a textured sample with clusters of atypical grains with the $\left[0\,1\,\overline{1}\,0\right]$ crystal direction aligned parallel with the TD of the sample. The randomly sampled grain orientations are plotted along with the low index crystal orientations from Fig. 3 in Fig. 9(a). The majority of the crystal orientations from the textured sample were found to have an occluded area fraction of 1.0 (Fig. 9(b)), which indicates that the there should be no channelling in these crystal orientations because there are no open channels available in the surface when the occluded area around each atom is taken into consideration. The occluded area fraction is high because there is no repeating lattice structure within the bulk depth simulated. There are therefore many unique atom positions in $x-y$ that increase the occluded area fraction. All the grain orientations from the textured sample have a linear density of 0.01 atoms Å^{-1} (Fig. 9(c)) because there was only one atom for each unique atom position in $x-y$ within the bulk depth used in the calculation of the linear density. If a deeper bulk were to be simulated ($>$ 400 Å), it is ex-

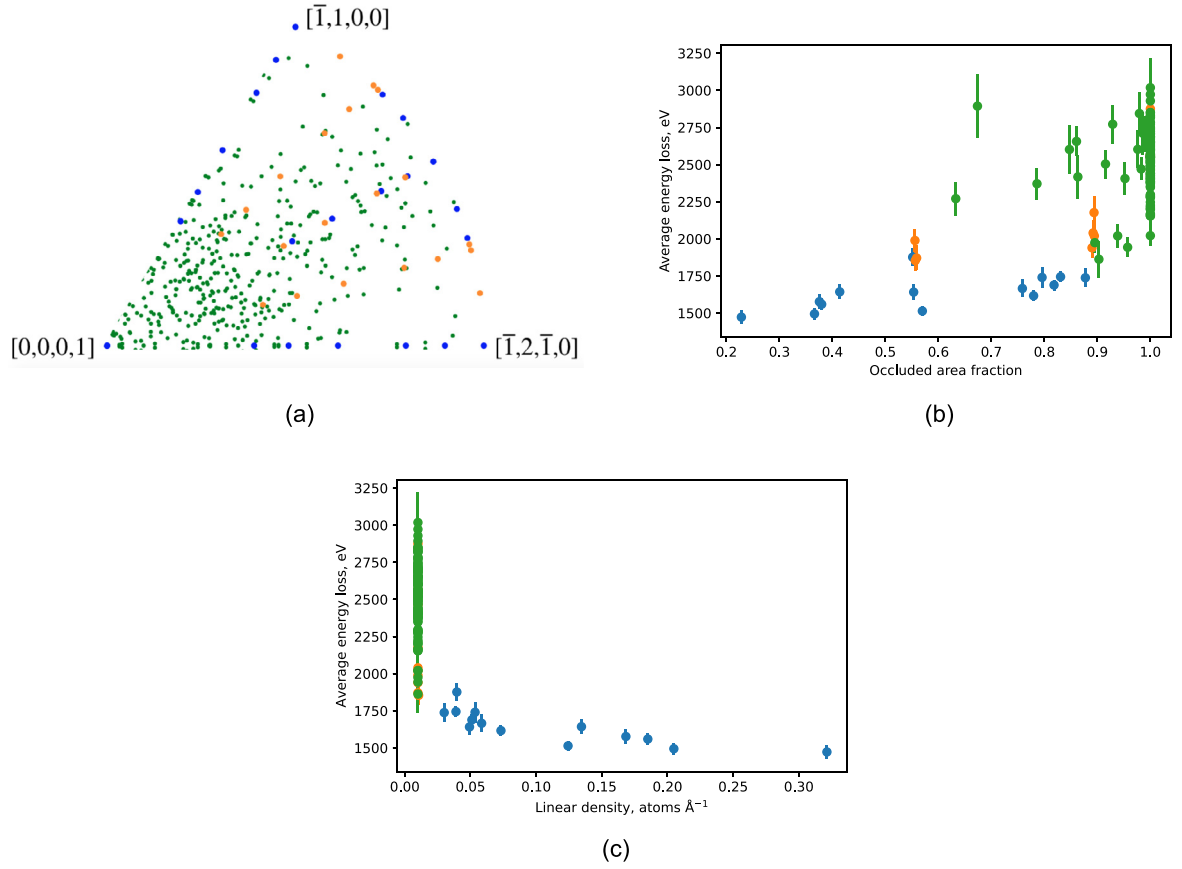

Fig. 9. The crystal orientations in Fig. 3 are shown in orange and blue and the 166 randomly sampled crystal orientations from the textured sample are plotted in green on the stereographic projection of the [0 0 0 1] crystal direction relative to the ND of the sample in (a). The average energy lost by the protons in each of the orientations is plotted as a function of (b) the occluded area density and (c) the linear density. The error bars represent the standard error of the average energy lost for the protons in each crystal orientation. (For interpretation of the references to color in this figure legend, the reader is referred to the web version of this article.)

pected that the linear density would increase because a repeating lattice structure would be expected within a larger bulk depth.

As a measure of the degree of channelling in the sampled crystal orientations, the average energy lost was converted into an indicative penetration depth i.e. the depth to which a proton will travel in a crystal before coming to rest. The indicative penetration depth, $\widetilde{R}$, can be calculated by converting the average energy loss into a stopping power, S, and assuming that the protons lose energy at a rate given by a viscous damping with a drag coefficient based on the average energy lost within the simulated depth of 200 Å:

$$\widetilde{R} = \frac{2E_0}{S}, \tag{6}$$

where E_0 is the ion's initial energy, which would be 2 MeV in this case and S was calculated by dividing the average energy lost by the protons for each orientation by the simulated depth of 200 Å.

After plotting each crystal orientation simulated on a (0 0 0 1) Zr plane pole figure, each point was coloured by the respective change in $\widetilde{R}$ as shown in Fig. 10(a). A linear interpolation was made between the sampled orientations to create a contour map (Fig. 10(a)) for the indicative penetration depths of protons in a Zr crystal.

The maximum $\widetilde{R}$ calculated in this work was found to be 28 µm deeper (71.8% higher) than the implantation depth for an amorphous Zr structure calculated using SRIM [5] as a result of channelling in the low-index direction $\left[\bar{1}\,2\,\bar{1}\,0\right]$. Whilst $\widetilde{R}$ is only an indicative penetration depth, we note that the mean $\widetilde{R}$ for all simulated crystal orientations is within 4% of the implantation depth for an amorphous Zr structure calculated using SRIM. This suggests that SRIM will significantly underestimate the penetration depth of ions where channelling occurs and therefore will not capture the correct damage distribution in a grain whose orientation encourages channelling.

Since many of the crystal orientations were sampled from a textured sample there is a high density of points within ±40° tilt from the ND of the sample. The majority of these orientations show a shallow penetration depth that is almost half that of the low index crystal directions like $\left[0\,1\,\bar{1}\,0\right]$ and $\left[\bar{1}\,2\,\bar{1}\,0\right]$.

As the crystal lattice is tilted so that the [0 0 0 1] crystal direction is more than 40° from the ND of the sample there are more crystal orientations which encourage proton channelling, hence the protons lose less energy and travel further into the crystal. As mentioned previously, when the TEM foil normal is aligned with the ND of the rolled plate (or the radial direction of the pilgered tube), *a*-loops can most easily be counted using atypically orientated grains i.e. with the [0 0 0 1] tilted ≥ 70° from the ND of the sample.

If an average is taken across the energy lost by protons in grains whose orientation are typical (≤ 40° from the ND of the sample) or atypical (≥ 70° from the ND of the sample) and then compared in Fig. 11 it can be seen that 10.3% less energy is lost in atypical grains compared with typical grains at 0 K.

Although the difference in the average energy lost in atypical grains compared with typical grains is small, the average energy lost in a single atypical grain varies more than the typical grain orientations as shown by the large standard deviation in Fig. 11 and the variation in $\widetilde{R}$ in Fig. 10(a). Hence by quantifying

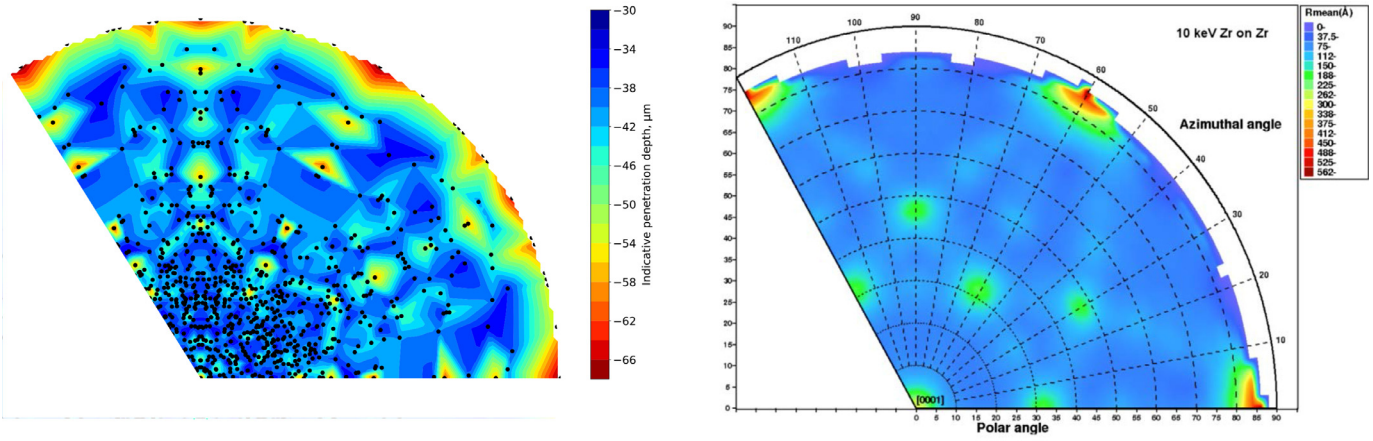

(a) (b)

Fig. 10. (a) The indicative penetration depths are plotted as a contour map on the (0 0 0 1) plane equal-area projection in Zr, where the [0 0 0 1] crystal direction is parallel with the ND of the sample. The black dots include the symmetrically equivalent points of the randomly sampled orientations from the textured sample and the low index crystal directions shown in Fig. 9(a). (b) is the penetration depth calculated by Nordlund et al. for 10 keV Zr into Zr [10].

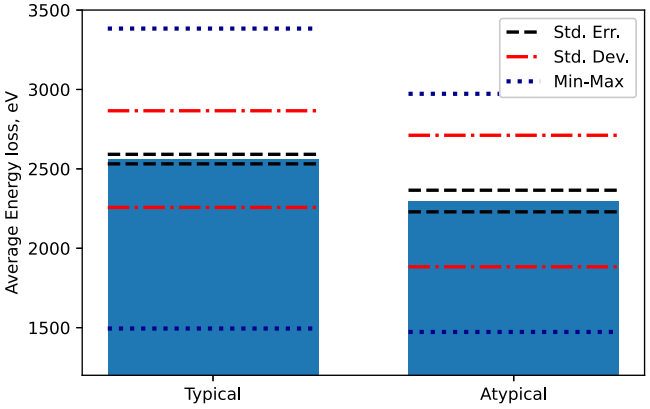

Fig. 11. A plot of the average energy lost by protons travelling in grains with the crystal direction [0 0 0 1] tilted $\leq 40^\circ$ from the ND of the sample (typical grain orientations) and grains with the crystal direction [0 0 0 1] is tilted $\geq 70^\circ$ from the ND of the sample (atypical grain orientations). The black dashed lines are the standard error, the red dot dash lines are the standard deviation in the average calculation of the average energy losses in the typical and atypical grains and the blue dotted lines shows the spread between the maximum and minimum average energy losses in the two grain classes. (For interpretation of the references to color in this figure legend, the reader is referred to the web version of this article.)

the damage in a sample using a single atypical grain orientation, the damage may vary by a factor of 2.

As mentioned previously there is already literature available for the channelling directions in Zr for 10 keV Zr [10], the results of which are reproduced in Fig. 10(b)[3]. Most notable in a comparison between Fig. 10(a) and (b) is that Fig. 10(b) is missing data at the 90° polar angle on the (0 0 0 1) pole figure. This is because the ions enter the crystal at oblique angles to the (0 0 0 1) planar surface when using the method in Nordlund et al.'s paper [10], hence many ions are back-scattered and do not enter the crystal. Instead the entire crystal surface must be rotated and a second pole figure plotted for the (2 $\bar{1}$ 1 0) planar surface to observe the penetration depth of ions into a lattice with the [0 0 0 1] crystal direction tilted by 90° from the ND of a sample. Meanwhile the spherical cluster method employed here can be used to simulate arbitrary crystal orientations and so the ion beam does not need to be tilted to access crystal orientations that have the [0 0 0 1] crystal direction at 90° from the ND of the sample and the ions do not need to enter at oblique angles. Instead all of the ions bombard perpendicular to the crystal surface.

Comparing Fig. 10(a) to (b), the positions of the largest penetration depths coincide for the low index crystal directions $[\bar{1}2\bar{1}0]$, $[\bar{2}203]$ and $[\bar{1}2\bar{1}3]$. These low index directions also coincide with the crystal orientations with low occluded area densities in Fig. 9(b). Unfortunately there are few grains with the $[\bar{1}2\bar{1}0]$ crystal orientation near parallel with the ND of the sample in the textured sample set shown in Fig. 9(a), hence the linear interpolation made between the sampled points has broadened the zones of highest penetration depths in Fig. 10(a) compared with Fig. 10(b). Apart from the $[\bar{1}2\bar{1}0]$, $[\bar{2}203]$ and $[\bar{1}2\bar{1}3]$ crystal orientations the penetration depths for the other crystal orientations are different, which could be for four reasons; the sampling of the orientations, the difference in lattice temperature and/or the mass and energy of the ion:

1. In this work 166 orientations were randomly taken from a textured sample, therefore there are a high number of data points clustered within ±40° tilt of the ND of the sample shown in Fig. 10(a). The linear interpolation between data points will therefore be a good approximation to the implantation depths for unknown orientations around the clustered points. There are fewer data points beyond 40° tilt therefore the linear interpolation may not adequately capture the change in implantation depth of protons in crystal orientations which are tilted more than 40° from the ND of the sample. This would explain the broad hot spots around the low index directions and why the small amount of channelling along the planes is not captured in Fig. 10(a) compared with Fig. 10(b).
2. The lattice was not thermalised in the simulations whereas Nordlund et al. [10] used a thermalised lattice at 300 K. Hence to investigate the effect of the lattice temperature on the channelling of protons we have repeated the simulations with a lattice thermalised to 300 K, 600 K, 900 K and 1200 K. The results are discussed in the next section.
3. In channelling theory, the mass of an ion does not alter which crystal orientations encourage channelling. However as found in the literature [10,35] the energy deposited in the crystal and the range that the ion travels change with the ion mass. For example Nordlund et al. [10] calculated that in theory the frac-

[3] Reprint used within the creative commons license 4.0 for Ref. [10]

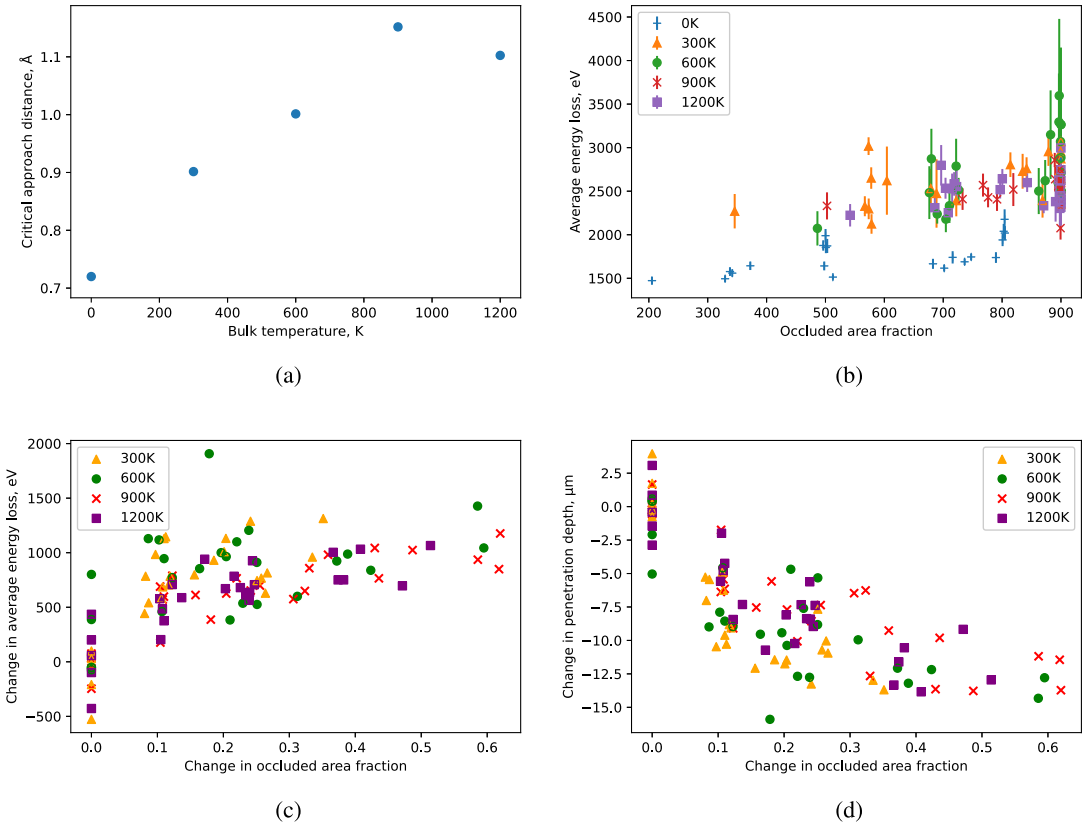

Fig. 12. (a) shows the change in the critical approach distance, ρ_{crit}, with the temperature of the lattice. (b) is a plot of the average energy lost by 2 MeV protons as function of occluded area fraction calculated for a lattice at 0 K, 300 K, 600 K, 900 K and 1200 K, using a screening centre=0.72 Å for the respective temperatures in (a). The error bars represent the standard error of the average energy lost for the protons in each crystal orientation and (c) shows the change in the average energy lost by 2 MeV protons in a thermalised lattice at 300 K, 600 K, 900 K and 1200 K as a function of the change in occluded area fraction from a non-thermalised lattice. (d) is the change in the penetration depth of the 2 MeV protons as a function of the change in occluded area fraction for the lattice thermalised to 300 K, 600 K, 900 K and 1200 K.

tion of ions that are channelled increases as the mass of the ion decreases but did not observe the expected change in the channelling fraction in their MD simulations. This effect however was not investigated further in Ref. [10]. In this work the simulated protons are 100× lighter than the Zr ions simulated in Ref. [10], therefore some of the crystal orientations may show a larger penetration depth in Fig. 10(a) compared with Fig. 10(b).

4. Along with the effect of the ion's mass, the ion's energy affects ρ_{crit}. As the ion's energy decreases ρ_{crit} must increase to find the regions of a channel where the high transverse energy (Eq. (2)) is conserved for low energy ions. Hence ρ_{crit} will be smaller for the high energy protons simulated in this work compared with the low energy ions simulated in Ref. [10]. The smaller ρ_{crit} means that a higher fraction of the 2 MeV protons are likely to be channelled compared with 10 keV ions and as such some crystal orientations will appear in Fig. 10(a) as crystal orientations that encourage channelling but may not appear on Fig. 10(b). To investigate the ion energy effect on channelling the low index crystal orientation simulations were repeated using 10 keV protons instead of 2 MeV. The results are discussed in Section 3.4.

3.3. Effect of temperature

In channelling theory the temperature of the lattice is expected to change the fraction of ions that are channelled because the vibration of atoms increases $E_{\perp}$. ρ_{crit} for a thermalised lattice must therefore increase to satisfy the conditions for channelling described above [23,24]. As the atoms are displaced from their equilibrium positions the effective area that the atoms occupy during a single vibration increases compared with an atom at 0 K. As the area occupied by an atom increases, the available space in the lattice for the protons to be channelled reduces. This can be seen by an increase in ρ_{crit} with the temperature of the lattice in Fig. 12(a), which is consistent with the observations of Ref. [23].

If the area fraction for each of the thermalised lattices is calculated using ρ_{crit} at 0 K (0.72 Å), the area fraction increases with the lattice temperature as a result of the atomic vibration as shown in Fig. 12(b).

In Fig. 12(c) the change in the occluded area fraction for the thermalised lattices compared with the equivalent occluded area fraction calculated for a non-thermalised lattice shows a corresponding increase in the average energy lost by 2 MeV protons. However the average energy lost for each crystal orientation does not seem to be dependent on the temperature of the lattice. On average the energy lost by protons travelling in a thermalised lattice increases by 500 eV but has no dependency with increasing lattice temperature above 300 K. Morgan et al. [23] discuss how the trajectory of channelled ions may become unstable after 200 Å because of the change in $E_{\perp}$ with the temperature of the lattice, at which point a large fraction of initially channelled ions may become dechannelled because of the increase in the probability of a nuclear interaction between the lattice atoms and the protons with increasing lattice vibrations. The bulk in this work was however only 200 Å deep therefore the different lattice vibrations for the thermalised lattices may not result in a large deviation in the energy lost by the protons, which may explain the lack of an increase in the average energy lost by protons with increasing lattice temperature.

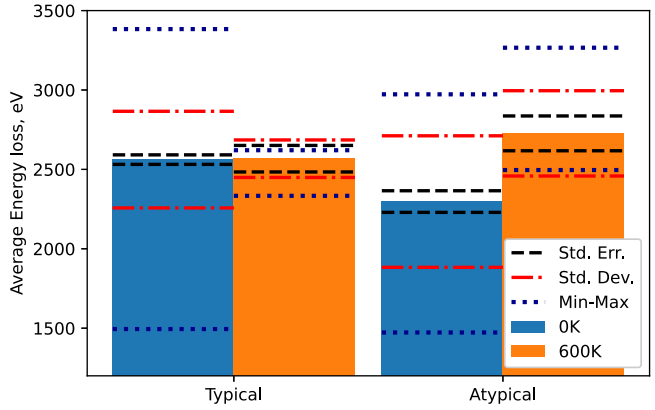

Fig. 13. The weighted average energy lost for typical grain orientations ($\leq 40^{\circ}$ from the ND of the sample) compared with the weighted average energy lost by 2 MeV protons travelling in atypical grain orientations ($\geq 70^{\circ}$ from the ND of the sample) at 600 K is compared with the average energy lost in typical and atypical grains at 0 K. The black dashed lines are the standard error, the red dot dash lines are the standard deviation in the average calculation of the average energy losses into the two grain classes and the blue dotted lines show the spread between the maximum and minimum average energy losses in the two grain classes. (For interpretation of the references to color in this figure legend, the reader is referred to the web version of this article.)

As mentioned previously proton irradiation is carried out at $\geq$ 600 K to simulate the temperature of a reactor and the damage in a proton-irradiated sample has in the past been quantified using atypically orientated grains [19,20]. To assess the effect of temperature on the damage measured in this way the average energy lost by protons travelling in atypical and typical thermalised lattices was weighted by the fractions of atypical and typical grains in the textured sample. The weighted average for the 600 K data is compared with the non-weighted 0 K data in Fig. 13. The averages for the 0 K data do not require any weighting as the 0 K simulations involved crystal orientations sampled randomly from a representative split-basal texture.

The trend in the average energy lost by protons in atypical and typical grains changes with the temperature of the lattice. Whereas less energy is lost on average in atypical grains compared with typical grains at 0 K, the reverse is found at 600 K. The average energy lost in typical grains only increases by 0.2% with an increase in lattice temperature whereas the average energy lost in atypical grains increases by 18.7% with the increase in lattice temperature.

The standard deviation is consistently larger in the atypical grains, at both lattice temperatures, than the typical grains because of the smaller number of grains (7.3%) in the split-basal texture that fall into the atypical grain category. The large deviation in the average energy lost in atypical grains compared with typical grains means that, on average, there is likely to be a large difference in the damage quantified in single atypical grains compared with typical grains, assuming that the average energy lost by protons in a grain correlates with the damage introduced into the grain. However, the reduction in standard deviation at 600 K compared with 0 K, suggests that the difference between atypical and typical grains is reduced at high temperatures.

With the limited number of crystal orientations simulated with a thermalised lattice it is difficult to discern whether the high average energy lost by protons in a thermalised lattice in Nordlund's work [10] (Fig. 10(b)) could explain the difference in the distribution of penetration depths calculated in this work as shown in Fig. 10(a). It is possible that the small standard deviation in the energy lost by protons travelling in thermalised lattices compared with non-thermalised lattices (Fig. 12(c)) would have resulted in tighter and fewer hot spots in Fig. 10(a) and may have instead been more similar to Fig. 10(b) had more crystal orientations been simulated.

3.4. Effect of ion energy

As discussed in Section 3.2, the differences in the distribution in $\tilde{R}$ (our proxy measure of range) between Fig. 10(a) and (b) could also be caused by the difference in the energy of the simulated ions. To investigate this possibility we now examine the results of simulations using 10 keV protons instead of 2 MeV protons.

Similar to the lattice temperature, channelling theory predicts an increase in ρ_{crit} as the ion's energy decreases to compensate for the increase in $E_{\perp}$ of the low energy ion. In this work ρ_{crit} for 10 keV protons was found to increase by 76% compared with ρ_{crit0} calculated for 2 MeV protons.

To compare the average energy lost by 10 keV protons with 2 MeV protons the occluded area fraction was calculated using ρ_{crit}= 0.72 Å and is shown in Fig. 14(a). The higher average energy lost by 10 keV can be explained by the larger fraction of the simulated protons that fall into the occluded regions of the lattice for 10 keV protons compared with 2 MeV protons as shown in Fig. 14(c). The fraction of the total protons that were channelled or scattered in each crystal orientation was calculated by finding whether ρ for each proton was separated less than the critical separation for the individual crystal orientation, ρ_{ci}, or more than ρ_{ci} respectively, where ρ_{ci} is the critical separation, calculated for each of the crystal orientations individually, using the same method as described in the methods section and in Section 3.1. Whilst the protons travelling through the different crystal orientations follow the same distribution as Fig. 6, the separation at which the increase in the energy loss occurs, as a result of high energy scattering events, can vary slightly for each crystal orientation because of the differing amounts of channelling in each lattice structure. A critical separation per crystal orientation was therefore used in this instance instead of ρ_{crit} found in Fig. 6.

The energy lost by 10 keV protons was found to increase on average by 49% compared with the average energy lost by 2 MeV protons travelling in the same crystal orientations (See Fig. 14(a)). The trend of increase in the energy lost with the occluded area fraction of the crystal orientation appears to be consistent for both ion energies.

The average energy lost by 10 keV protons travelling in the [0 0 0 1] and $\left[\bar{1}\,2\,\bar{1}\,0\right]$ crystal directions was converted into an effective range (Eq. (6)) and compared with the penetration depth for the same crystal directions from Nordlund's work [10] in Fig. 10(b). The energy lost by 10 keV protons travelling in [0 0 0 1] simulated in this work resulted in $\tilde{R}$ that was 11$\times$ larger than the penetration depth in Fig. 10(b) and the $\tilde{R}$ calculated in this work for the $\left[\bar{1}\,2\,\bar{1}\,0\right]$ crystal direction was 5$\times$ larger than the equivalent in Fig. 10(b). As mentioned at the end of Section 3.2, the ion mass can change the energy deposited in the grain and the range of the ion, which appears to be the cause of the smaller average energy lost by the protons simulated in this work compared with the Zr ions simulated in Ref. [10].

The smaller average energy lost by low energy protons in this work compared with Nordlund's work in Ref. [10] and the difference in the distribution of penetration depths between Fig. 10(a) and (b) suggests that the most likely cause of the disagreement is the lattice temperature and the ion mass rather than the ion energy.

4. Impact on future studies

Throughout this paper, we have considered the common experimental practice of preparing samples to observe the microstructural changes caused by irradiation in textured samples. In this

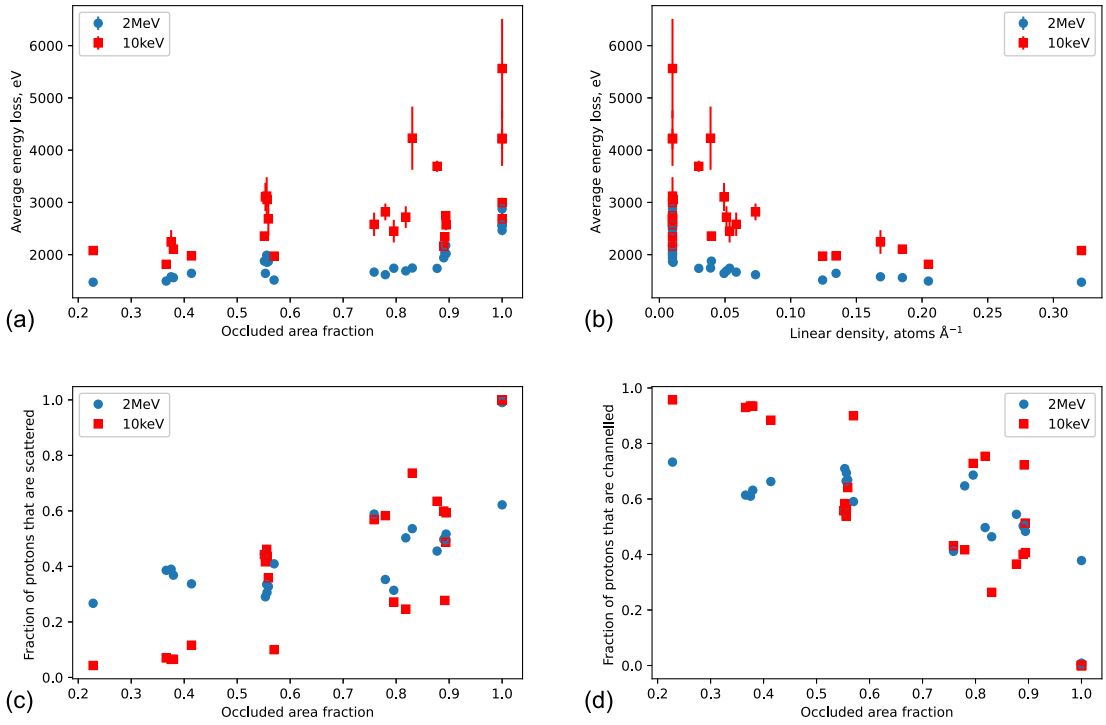

Fig. 14. The average energy lost by 2 MeV protons compared with 10 keV is plotted as function of (a) the occluded area fraction and (b) the linear density of the simulated crystal orientations shown in Fig. 3. The fraction of the total number of protons simulated per crystal orientation that are either (c) scattered or (d) channelled is plotted as a function of occluded area fraction for protons simulated with 2 MeV and 10 keV kinetic energy. Whether a proton is classed as being scattered or channelled is determined by the proton's separation from the nearest lattice atom relative to the critical separation for the individual crystal orientation, ρ_{ci}, i.e. a proton is considered channelled if $\rho \geq \rho_{ci}$ and scattered if $\rho < \rho_{ci}$.

section we summarise the key points that might impact future experimental studies of irradiated samples.

First we note that the difference in energy loss (and therefore the likely difference in damage) between the *average* typical and the *average* atypical grain is rather small. This is because although the zirconium alloys used in fuel clad have a strong texture, there is still considerable spread in the orientation of the basal poles amongst the typical grains and channelling is only appreciable when the proton beam is closely aligned with a low index direction. Therefore we conclude that the suitability of proton irradiation as a surrogate for neutron irradiation is not detrimentally affected by channelling.

Second, as a caveat to the above statement, we note that we do predict a large grain-to-grain variation in the energy loss as a function of grain orientation. Therefore an evaluation of damage in a proton irradiation experiment that examines only a small number of grains may not be representative of the average grain. Hence we conclude that whilst channelling has a small effect *on average* it can have a large effect on the damage in any given grain.

Third, to guard against incorrect conclusions from studies based on a small number of grains, we have shown that the energy deposited is strongly correlated with the occluded area fraction. This observation provides a means of assessing the individual grains included in an experimental TEM study to determine the extent to which they may be poorly representative of average behaviour. If the orientation of the proton beam relative to the sample is known, then those grains likely to show anomalously large channelling effects can be identified.

5. Conclusions

This paper reports the results of our simulations of the interactions between protons and Zr bulk using the molecular dynamics code LAMMPS [26]. We have examined how the degree of proton channelling changes with the orientation of a crystal as well as the effect of the ion energy and the temperature of the lattice on the energy deposited by protons in bulk Zr. As previously described, atypical grains can be chosen to quantify the damage in a proton-irradiated sample because of the increase in contrast in TEM when viewing *a*-type dislocation loops. The choice of a specific texture component should however be made with regard to the effects of proton channelling on the energy deposition in grains [19,20]. We have determined what may be the consequences of using atypical grains to quantify the damage from proton irradiation in a textured sample. In summary, we conclude that:

- The average energy lost by 2 MeV protons can change with the orientation of the Zr crystal by up to 40%.
- The degree of channelling from grain to grain changes the energy lost by protons and can result in losses that differ by a factor of 2 between grains. Hence quantifying the damage in an irradiated sample using a single grain, or a small number of grains, will give results that may not be representative of the damage in a textured polycrystalline sample.

Furthermore, we conclude that:

- The average energy lost by protons increases with the calculated occluded area fraction per crystal orientation. The occluded area fraction may be an easily calculated predictor of the degree of proton channelling with changing crystal orientation without the need to solve analytical equations from channelling theory.
- The average energy lost by protons increases by 49% with decreasing ion energy from 2 MeV to 10 keV.
- Protons travelling through thermalised and non-thermalised bulks with low index crystal orientations like $[\bar{1}2\bar{1}0]$ and $[0\,1\,\bar{1}\,0]$ show a high degree of channelling. However the thermalised lattice increased the number of scattering events and

increased the energy lost by protons (500 eV) compared with a lattice at 0 K.
- The average energy lost by protons increased by 38% in a thermalised lattice of 300 K compared with a lattice at 0 K. There was however no noticeable further increase in the average energy lost in lattices with increasing temperature beyond 300 K, most likely because of the thin simulation bulk used in this work.
- We compared our work with Ref. [10] and found discrepancies between the results, namely in which of the crystal orientations encourage the smallest amount of energy loss as a result of channelling. We conclude that this was mainly due to the difference in the temperature of the lattices simulated.
- When the energy lost by high energy protons is instead averaged across many grains, there is little difference in the energy lost by protons, for example 10.3% less energy being lost in atypical compared with typical grains.
- The difference in the energy lost by protons travelling in atypical grains compared with typical grains is reduced with increased lattice temperature (>300 K). At 600 K 6.2% more energy is lost by protons in atypical grains compared with typical grain orientations.
- The change in trend between the average energy lost in atypical and typical grains with lattice temperature is because of the variability (34% at 0 K and 10% at 600 K) in the energy lost within individual crystal orientations.
- The large deviation in the average energy lost in atypical grains compared with typical grains means that, on average, there is unlikely to be much of a difference observed in the damage quantified in atypical grains compared with typical grains at high temperatures.
- Since proton irradiation experiments are carried out at 600 K, the damage quantified using atypical grains can be representative of the damage in a textured sample, if the damage has been averaged over many atypical grains.

Declaration of Competing Interest

The authors declare that they have no known competing financial interests or personal relationships that could have appeared to influence the work reported in this paper.

CRediT authorship contribution statement

A. Adrych-Brunning: Conceptualization, Methodology, Software, Validation, Formal analysis, Investigation, Data curation, Writing - original draft, Visualization, Project administration. **C.P. Race:** Conceptualization, Resources, Data curation, Writing - review & editing, Supervision, Project administration, Funding acquisition.

Acknowledgements

The authors wish to thank Maria Yankova for the development of a comprehensive python package to create pole figure plots as well as Rhys Thomas for the data collected for a textured sample of Zr. The authors would also like to acknowledge the assistance given by IT Services and the use of the Computational Shared Facility at The University of Manchester. A. Adrych-Brunning was funded by EPSRC Centre for Doctoral Training in Nuclear Energy - Next Generation Nuclear [grant number EP/LO15390/1] with additional sponsorship by Jacobs (formerly Wood).

C. P. Race was funded by a University Research Fellowship of the Royal Society.

References

[1] E. Tenckhoff, Deformation Mechanisms, Texture, and Anisotropy in Zirconium and Zircaloy, ASTM Technical publication (STP 966), 1988, doi:10.1017/CBO9781107415324.004.
[2] R. Qiu, Z. Song, B. Luan, Q. Yue, L. Wang, G. Yuan, K. Linga Murty, Q. Liu, Evolution of microstructure and second-phase particles in Zr-Sn-Nb-Fe alloy tube during Pilger processing, J. Nucl. Sci. Technol. 54 (12) (2017) 1321–1329, doi:10.1080/00223131.2017.1365023.
[3] B.A. Cheadle, C.E. Ells, W. Evans, The development of texture in zirconium alloy tubes, J. Nucl. Mater. 23 (2) (1967) 199–208, doi:10.1016/0022-3115(67)90065-7.
[4] A. Melcher, A. Unser, M. Reichhardt, B. Nestler, Conversion of EBSD data by a quaternion based algorithm to be used for grain structure simulations, Tech. Mech. 30 (4) (2009) 401–413.
[5] J.F. Ziegler, M.D. Ziegler, J.P. Biersack, SRIM – The stopping and range of ions in matter (2010), Nucl. Instrum. Methods Phys. Res. Sect. B Beam Interact. Mater. Atoms 268 (11-12) (2010) 1818–1823, doi:10.1016/j.nimb.2010.02.091.
[6] G. Dearnaley, The channelling of ions through silicon detectors, IEEE Trans. Nucl. Sci. (1964) 249.
[7] G.R. Piercy, F. Brown, J.A. Davies, M. McCargo, Experimental evidence for the increase of heavy ion ranges by channeling in crystalline structure, Phys. Rev. Lett. 10 (9) (1963) 399–400, doi:10.1103/PhysRevLett.10.399.
[8] B. Domeij, F. Brown, J.A. Davies, G.R. Piercy, E.V. Kornelsen, Anomalous penetration of heavy ions of keV energies in monocrystalline tungsten, Phys. Rev. Lett. 12 (13) (1964) 363–366, doi:10.1103/PhysRevLett.12.363.
[9] M.T. Robinson, O.S. Oen, Computer studies of the slowing down of energetic atoms in crystals, Phys. Rev. 132 (6) (1963) 2385–2398, doi:10.1103/PhysRev.132.2385.
[10] K. Nordlund, F. Djurabekova, G. Hobler, Large fraction of crystal directions leads to ion channeling, Phys. Rev. B 94 (21) (2016) 214109, doi:10.1103/PhysRevB.94.214109.
[11] K. Nordlund, Molecular dynamics simulation of ion ranges in the 1-100 keV energy range, Comput. Mater. Sci. 3 (4) (1995) 448–456, doi:10.1016/0927-0256(94)00085-Q.
[12] C. Cohen, D. Dauvergne, High energy ion channeling: Principles and typical applications, Nucl. Instrum. Methods Phys. Res. Sect. B Beam Interact. Mater. Atoms 225 (1-2 SPEC. ISS.) (2004) 40–71, doi:10.1016/j.nimb.2004.03.017.
[13] G.S. Was, J.T. Busby, T. Allen, E.A. Kenik, A. Jensson, S.M. Bruemmer, J. Gan, A.D. Edwards, P.M. Scott, P.L. Andreson, Emulation of neutron irradiation effects with protons: validation of principle, J. Nucl. Mater. 300 (2-3) (2002) 198–216, doi:10.1016/S0022-3115(01)00751-6.
[14] G.S. Was, Z. Jiao, E. Getto, K. Sun, A.M. Monterrosa, S.A. Maloy, O. Anderoglu, B.H. Sencer, M. Hackett, Emulation of reactor irradiation damage using ion beams, Scr. Mater. 88 (2014) 33–36, doi:10.1016/j.scriptamat.2014.06.003.
[15] D.O. Northwood, et al., Characterization of neutron irradiation damage in zirconium alloys - an international "round-robin" experiment, J. Nucl. Mater. 79 (2) (1979) 379–394, doi:10.1016/0022-3115(79)90103-X.
[16] R.A. Holt, Mechanisms of irradiation growth of α-zirconium alloys, J. Nucl. Mater. 159 (1988) 310–338, doi:10.1016/0022-3115(88)90099-2.
[17] C.H. Woo, Theory of irradiation deformation in non-cubic metals: effects of anisotropic diffusion, J. Nucl. Mater. 159 (1988) 237–256, doi:10.1016/0022-3115(88)90096-7.
[18] A. Harte, D. Jädernäs, M. Topping, P. Frankel, C.P. Race, J. Romero, L. Hallstadius, E.C. Darby, M. Preuss, The effect of matrix chemistry on dislocation evolution in an irradiated Zr alloy, Acta Mater. 130 (2017) 69–82, doi:10.1016/j.actamat.2017.03.024.
[19] A. Harte, M. Topping, P. Frankel, D. Jädernäs, J. Romero, L. Hallstadius, E.C. Darby, M. Preuss, Nano-scale chemical evolution in a proton -and neutron-irradiated Zr alloy, J. Nucl. Mater. 487 (2017) 30–42.
[20] M. Topping, A. Harte, P. Frankel, C. Race, G. Sundell, The effect of iron on dislocation evolution in model and commercial zirconium alloys, in: Zirconium in the Nuclear Industry: 18th International Symposium, ASTM, 2018, pp. 796–822, doi:10.1520/STP159720160068.
[21] A.K. Revelly, N. Srinivasan, A.S. Panwar, K.V. Mani Krishna, R. Tewari, D. Srivastava, G.K. Dey, I. Samajdar, Orientation sensitivity of focused ion beam damage in pure zirconium: direct experimental observations and molecular dynamics simulations, Philos. Mag. 94 (14) (2014) 1601–1621, doi:10.1080/14786435.2014.892220.
[22] J. Lindhard, Influence of crystal lattice on motion of energetic charged particles, Mat. Fys. Medd. Dan. Vid. Selsk. 34 (1965) 1–64.
[23] D.V. Morgan, D.V. Vliet, Critical approach distances and critical angles for channelling, Radiat. Eff. 8 (1-2) (1971) 51–61, doi:10.1080/00337577108231009.
[24] G. Hobler, Critical angles and low-energy limits to ion channeling in silicon, Radiat. Eff. Defects Solids 139 (1) (1996) 21–85, doi:10.1080/10420159608212927.
[25] M. Christensen, W. Wolf, C. Freeman, E. Wimmer, R.B. Adamson, L. Hallstadius, P.E. Cantonwine, E.V. Mader, Diffusion of point defects, nucleation of dislocation loops and effect of hydrogen in hcp-Zr: Ab initio and classical simulations, J. Nucl. Mater. 460 (2015) 82–96, doi:10.1016/j.jnucmat.2015.02.013.
[26] S. Plimpton, Fast parallel algorithms for short-range molecular dynamics, J. Comput. Phys. 117 (1995) 1–19, doi:10.1006/jcph.1995.1039.
[27] B.J. Lee, S.H. Choi, Computation of grain boundary energies, Model. Simul. Mater. Sci. Eng. 12 (2004) 621–632, doi:10.1088/0965-0393/12/4/005.
[28] C.P. Race, D.R. Mason, M.W. Finnis, W.M.C. Foulkes, A.P. Horsfield, A.P. Sutton, The treatment of electronic excitations in atomistic models of radia-

tion damage in metals, Reports Prog. Phys. 73 VN - r (11) (2010) 116501, doi:10.1088/0034-4885/73/11/116501.
[29] M.W. Finnis, P. Agnew, A.J.E. Foreman, Thermal excitation of electrons in energetic displacement cascades, Phys. Rev. B 44 (2) (1991) 567–574, doi:10.1103/PhysRevB.44.567.
[30] A. Caro, A.A. Correa, A. Tamm, G.D. Samolyuk, G.M. Stocks, Adequacy of damped dynamics to represent the electron-phonon interaction in solids, Phys. Rev. B - Condens. Matter Mater. Phys. 92 (14) (2015) 1–7, doi:10.1103/PhysRevB.92.144309.
[31] A. Caro, M. Victoria, Ion-electron interaction, Phys. Rev. A 40 (5) (1989).
[32] D.M. Duffy, A.M. Rutherford, Including the effects of electronic stopping and electron-ion interactions in radiation damage simulations, J. Phys. Condens. Matter 19 (1) (2007) 16207, doi:10.1088/0953-8984/19/1/016207.
[33] D.R. Mason, J. le Page, C.P. Race, W.M.C. Foulkes, M.W. Finnis, A.P. Sutton, Electronic damping of atomic dynamics in irradiation damage of metals, J. Phys. Condens. Matter 19 (2007) 436209, doi:10.1088/0953-8984/19/43/436209.
[34] C.P. Race, D.R. Mason, M.H.F. Foo, W.M.C. Foulkes, A.P. Horsfield, A.P. Sutton, Quantum-classical simulations of the electronic stopping force and charge on slow heavy channelling ions in metals., J. Phys. Condens. Matter 25 (12) (2013) 125501, doi:10.1088/0953-8984/25/12/125501.
[35] L.P. Zheng, Z.Y. Zhu, Y. Li, D.Z. Zhu, H.H. Xia, Ion mass dependence for low energy channeling in single-wall nanotubes, 2008, 10.1016/j.nimb.2008.01.001